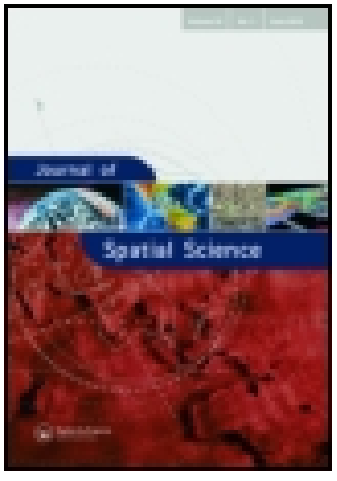
This article was downloaded by: [RMIT University]
On: 18 February 2015, At: 15:23
Publisher: Taylor & Francis
Informa Ltd Registered in England and Wales Registered Number: 1072954 Registered office: Mortimer House, 37-41 Mortimer Street, London W1T 3JH, UK



CrossMark
Click for updates

Journal of Spatial Science
Publication details, including instructions for authors and subscription information:
http://www.tandfonline.com/loi/tjss20

Using the Geoscience Australia-CSIRO ASTER maps and airborne geophysics to explore Australian geoscience

R. Hewson[a], D. Robson[b], A. Mauger[c], T. Cudahy[d], M. Thomas[e] & S. Jones[a]

[a] School of Mathematical & Geospatial Sciences, RMIT University, Melbourne, Australia

[b] NSW Trade & Investment, Maitland, Australia

[c] SA Department for Manufacturing, Innovation, Trade, Resources and Energy, Adelaide, Australia

[d] CSIRO Earth Science & Resource Engineering, Perth, Australia

[e] Geoscience Australia, Canberra, Australia

Published online: 16 Feb 2015.

To cite this article: R. Hewson, D. Robson, A. Mauger, T. Cudahy, M. Thomas & S. Jones (2015): Using the Geoscience Australia-CSIRO ASTER maps and airborne geophysics to explore Australian geoscience, Journal of Spatial Science, DOI: 10.1080/14498596.2015.979891

To link to this article: http://dx.doi.org/10.1080/14498596.2015.979891

PLEASE SCROLL DOWN FOR ARTICLE

Taylor & Francis makes every effort to ensure the accuracy of all the information (the "Content") contained in the publications on our platform. However, Taylor & Francis, our agents, and our licensors make no representations or warranties whatsoever as to the accuracy, completeness, or suitability for any purpose of the Content. Any opinions and views expressed in this publication are the opinions and views of the authors, and are not the views of or endorsed by Taylor & Francis. The accuracy of the Content should not be relied upon and should be independently verified with primary sources of information. Taylor and Francis shall not be liable for any losses, actions, claims, proceedings, demands, costs, expenses, damages, and other liabilities whatsoever or howsoever caused arising directly or indirectly in connection with, in relation to or arising out of the use of the Content.

This article may be used for research, teaching, and private study purposes. Any substantial or systematic reproduction, redistribution, reselling, loan, sub-licensing, systematic supply, or distribution in any form to anyone is expressly forbidden. Terms &

Conditions of access and use can be found at http://www.tandfonline.com/page/terms-and-conditions

Downloaded by [RMIT University] at 15:23 18 February 2015

Journal of Spatial Science, 2015
http://dx.doi.org/10.1080/14498596.2015.979891

Taylor & Francis
Taylor & Francis Group

Using the Geoscience Australia-CSIRO ASTER maps and airborne geophysics to explore Australian geoscience

R. Hewson[a]*, D. Robson[b], A. Mauger[c], T. Cudahy[d], M. Thomas[e] and S. Jones[a]

[a]*School of Mathematical & Geospatial Sciences, RMIT University, Melbourne, Australia;* [b]*NSW Trade & Investment, Maitland, Australia;* [c]*SA Department for Manufacturing, Innovation, Trade, Resources and Energy, Adelaide, Australia;* [d]*CSIRO Earth Science & Resource Engineering, Perth, Australia;* [e]*Geoscience Australia, Canberra, Australia*

Downloaded by [RMIT University] at 15:23 18 February 2015

This study evaluated the geological mapping potential of the recently released Australian CSIRO-GA ASTER satellite geoscience products in providing mineral abundance and compositional information. A range of environments was examined by using test sites including the temperate cultivated New South Wales area of Wagga Wagga, and the semi-arid rangeland Mt Fitton of South Australia. Data integration of the ASTER derived products was undertaken with geophysical data, digital elevation models and fractional vegetation cover information. The study demonstrated that these products can successfully assist geological mapping within semi-arid areas and, to a lesser extent, within temperate open woodland environments.

Keywords: Wagga Wagga; Mt Fitton; ASTER; mineralogy; geology; DEMs; geophysics

1. Introduction

In August 2012 a series of 17 compositional Australia-wide map products was released by the Commonwealth Scientific Industrial Research Organisation (CSIRO) and Geoscience Australia (GA) from imagery obtained by the multispectral satellite sensor, Advanced Spaceborne Thermal Emission Reflectance Radiometer (ASTER) (Cudahy 2012). This followed many successful years of data acquisition by ASTER following its development by Japan's Ministry of Economy, Trade and Industry (METI) and launch by the National Aeronautics and Space Administration (NASA) (Yamaguchi *et al.* 2001). These compositional maps offer the opportunity of new 'eyes' for regional geological mapping within Australia to assist exploration activities.

This particular study aims to examine the capabilities of the Australian ASTER map products within two different environments encompassing the temperate and cultivated Wagga Wagga 1:100,000 (100 K) map sheet of New South Wales (NSW), and the semi-arid Mt Fitton area of South Australia (SA). Wagga Wagga was examined in particular in conjunction with traditional airborne magnetic, radiometric and digital elevation model (DEM) datasets acquired by the Geological Survey of New South Wales (GSNSW). Another objective of this study was to examine the robustness of the geoscience mapping capabilities of ASTER, as individual map

*Corresponding author. Email: robert.hewson@rmit.edu.au

© The work of D. Robson, A. Mauger, T. Cudahy, and M. Thomas was authored as part of their official duties as an Employee of the Australian Government and is therefore Crown Copyright 2015.
R. Hewson and S. Jones hereby waive their right to assert copyright, but not their right to be named as co-authors in the article.

products, and via data integration, within two different environments of Australia. This study also follows the previous presentation at the 2013 Australian Society of Exploration Geophysicists conference (Hewson *et al.* 2013). A more detailed description of the Wagga Wagga 100 K imagery, field data and its analysis is found in Hewson (2013).

ASTER multispectral satellite sensor

ASTER acquires imagery within a 60 km × 60 km scene area from 14 different spectral bands with a pixel resolution of between 15 m and 90 m, depending on whether they were generated by the Visible–Near Infrared (VNIR), Shortwave Infrared (SWIR) or Thermal Infrared (TIR) sensors (Yamaguchi *et al.* 2001) (Table 1).

ASTER tracks a similar Earth orbit and altitude to the older Landsat TM satellites, with similar VNIR bands (minus band 1) but with five additional SWIR bands, providing higher spectral resolution than Landsat TM's band 7 (Figure 1). ASTER also measures radiance using five bands within the TIR wavelength region (8–12 μm) (Figure 1), providing the first access to civilian multispectral TIR data at moderate spatial resolution (90 m).

The additional bands of ASTER, compared with Landsat, provide an improved capability to discriminate and potentially identify the surface vegetation and rock/soil composition. An overview of and comparison between the characteristics of ASTER, Landsat and other current satellite sensors were described by Michael (2012). In particular, the additional ASTER SWIR bands can detect the clay mineral absorption signature (e.g. sandstone in Figure 1) separately from the carbonate absorption signature (e.g. limestone in Figure 1). ASTER's TIR bands can also discriminate quartz and silica-bearing rocks (e.g. sandstone, soil in Figure 1) by their absorption features in the 8–10 μm range. The ability of ASTER's VNIR, SWIR and TIR 14-band multispectral sensor to detect diagnostic absorption signatures of outcropping minerals (groups) is determined by its spectral resolution (i.e. bandwidth), specific wavelengths measured (Figure 1) and also its ground spatial resolution (Table 1).

Mineral detection using ASTER

The use of ASTER satellite data products follows several decades of laboratory-based spectroscopy within the VNIR, SWIR and TIR wavelength regions for the measurement of minerals and mineral groups (Vincent & Thomson 1972; Hunt & Ashley 1979). In particular, the ferric oxide group

Table 1. Spectral bandwidths and central band wavelengths of the ASTER sensor (Fujisada *et al.* 1998)

Module	VNIR	SWIR	TIR
Spectral Bandwidth (μm) [Centre λ (μm)]	Band 1 0.52–0.60 [0.556]	Band 4 1.600–1.700 [1.656]	Band 10 8.125–8.475 [8.291]
	Band 2 0.63–0.69 [0.661]	Band 5 2.145–2.185 [2.167]	Band 11 8.475–8.825 [8.634]
	Band 3N 0.78–0.86 [0.807]	Band 6 2.185–2.225 [2.209]	Band 12 8.925–9.275 [9.075]
	Band 3B 0.78–0.86 [0.804] (Backward looking)	Band 7 2.235–2.285 [2.262]	Band 13 10.25–10.95 [10.657]
		Band 8 2.295–2.395 [2.336]	Band 14 10.95–11.65 [11.318]
		Band 9 2.360–2.430 [2.400]	
Spatial Resolution (m)	15	30	90

Downloaded by [RMIT University] at 15:23 18 February 2015

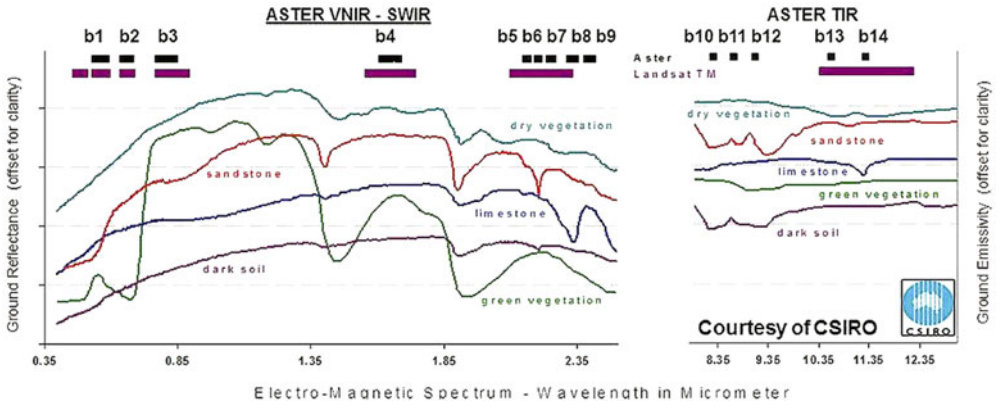


Figure 1. Typical reflectance and emissivity signatures, and their comparison with ASTER and Landsat TM spectral bands (e.g. bands: 'bx').

Downloaded by [RMIT University] at 15:23 18 February 2015

(e.g. hematite and goethite), OH- bearing minerals (e.g. clays, micas, amphiboles) and other silicates have been shown to display diagnostic signatures within the VNIR, SWIR and TIR wavelength regions, respectively (Sherman 1985; Clark *et al.* 1990; Grove *et al.* 1992; Salisbury & D'Aria 1992). Such spectral signatures exhibit absorption features whose depth in reflectance values (or emissivity within the TIR) can be approximately related to abundance or content of that mineral. Some mineral signatures (e.g. mica) also demonstrate shifts in the wavelength of their absorption reflectance minima (approximately 2200 nm) associated with compositional chemistry changes. Such inferred compositional changes of mica can be relevant for the interpretation of their possible metamorphic or alteration history (Duke 1994).

The effect of the ASTER sensor spectral resolution on its ability to detect and discriminate different minerals within common rock units and soils can be demonstrated by re-sampling laboratory-measured mineral signatures into equivalent 14-band ASTER signatures (Hewson 2013). In particular, the laboratory acquired USGS VNIR-SWIR and Johns Hopkins University (JHU) TIR spectral libraries (Clark *et al.* 1990; Salisbury & D'Aria 1992) were re-sampled to ASTER VNIR-SWIR and TIR band resolutions (Table 1) (Figures 2a, b, 3). The chlorophyll 'red edge' of green vegetation is distinguished from dry vegetation at ASTER VNIR resolution (bands 2 and 3, e.g. 660 nm and 800 nm; Figure 2a), as with traditional Landsat spectral observations. Ferric iron oxide minerals, goethite and hematite, also display some spectral difference within the VNIR (e.g. ASTER band 1, 550 nm). AlOH (clay group) minerals, such as muscovite and kaolinite, have diagnostic absorption features within the SWIR wavelength region between 2100 to 2250 nm that can be discriminated by ASTER (bands 5–7, Figure 2b). Similarly, MgOH/carbonate group minerals (e.g. chlorite, dolomite) have SWIR diagnostic absorption features between 2250 and 2400 nm (ASTER bands 7–9). At ASTER spectral resolution these diagnostic spectral signatures are less precise than laboratory measurements, although they provide qualitative to semi-quantitative mineral information. Overall ASTER's VNIR and SWIR sensors show themselves capable of discriminating and generally identifying broad mineral groups such as ferric iron oxide, AlOH and MgOH/carbonate.

In addition to the nine bands in the VNIR-SWIR region, ASTER also has five thermal

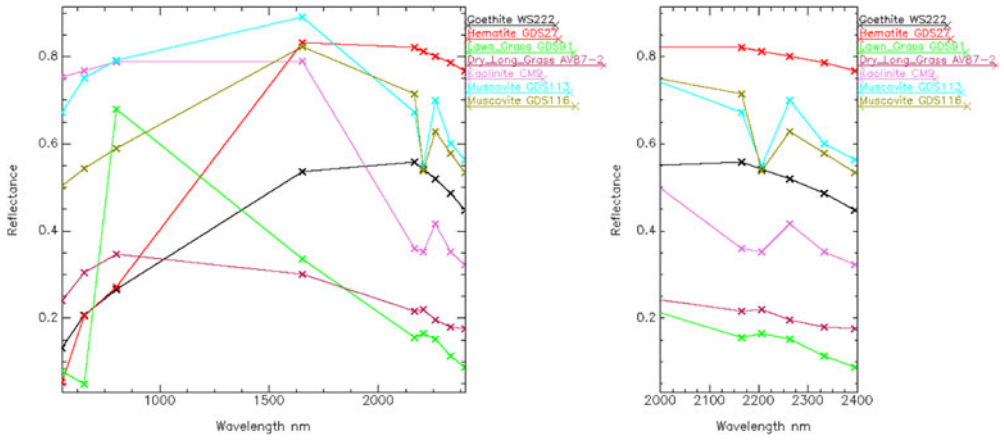


Figure 2. (a) VNIR to SWIR spectral reflectance signatures of ferric oxide, AlOH group minerals and of typical vegetation spectra, resampled to ASTER resolution; (b) detailed SWIR view of (a). Courtesy of the USGS VNIR-SWIR spectral library (Clark *et al.* 1990).

bands for mapping silicates. Resampling the JHU spectral library to ASTER resolution indicates the potential of discriminating quartz and silicate minerals (Figure 3). In particular, ASTER TIR bands 10, 11 and 13 (8.3 μm, 8.6 μm, 9.1 μm respectively) are shown to be sensitive to the quartz spectral reststrahlen feature between 8.0 and 9.5 μm (Figure 3).

Past ASTER geological case studies

There have been several successful geological mapping case studies undertaken using

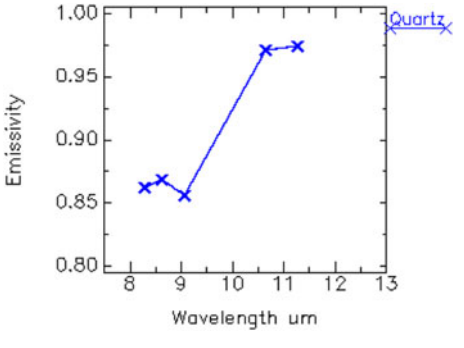


Figure 3. TIR spectral emissivity signature of quartz resampled to ASTER spectral resolution. Courtesy of the JHU spectral library (Salisbury & D'Aria 1992).

ASTER since its launch in 1999. Studies within the semi-arid terrain of Mt Fitton in the northern Flinders Ranges of South Australia established ASTER's ability to discriminate the minerals associated with the major lithological units and also areas of alteration (Hewson *et al.* 2001). Rowan and Mars (2003) also showed early on that lithological mapping was feasible in areas of good exposure. Hewson *et al.* (2005) at Broken Hill, NSW, demonstrated simple devised spectral indices (*e.g.* band ratios) using ASTER radiance imagery to map mineralogy. This approach was based on the Relative Band Depth (Crowley *et al.* 1989) ratio algorithm, which targets the spectral reflectance absorption features, where the content or abundance of a mineral (or mineral group) is based on its depth relative to the shoulders ('White mica', Figure 4). Variations within mineral groups, such as AlOH or white mica, were also interpreted by examining ratios such as R_{b7}/R_{b5}. (Hewson *et al.* 2005) (Figure 4).

Such indices are an attempt to represent compositional changes such as those previously identified by shifts in the minima wavelength of the mica absorption between 2.19 and 2.21 μm (Duke 1994). Limitations to

Downloaded by [RMIT University] at 15:23 18 February 2015

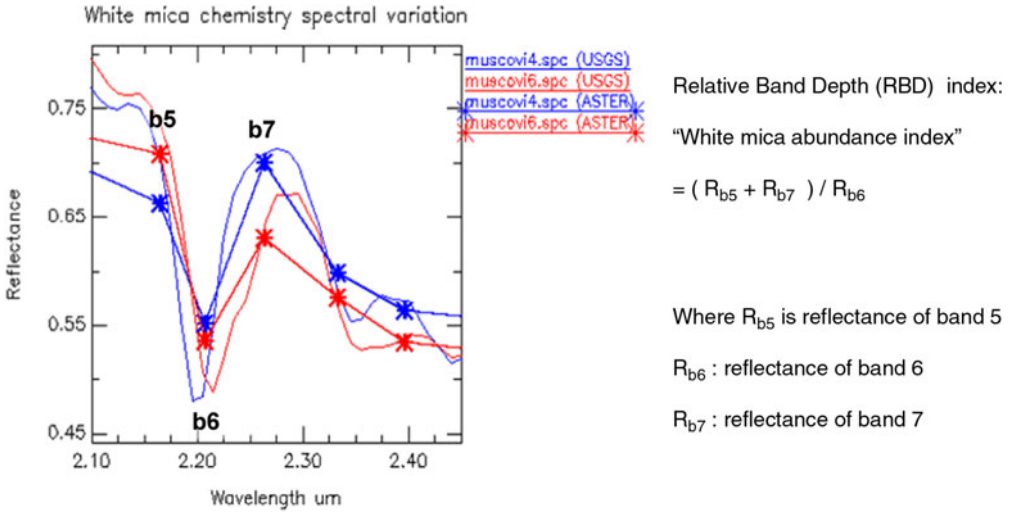


Figure 4. Laboratory-measured AlOH or mica spectra and their ASTER resampled equivalent signature, highlighting spectral indices to represent content and compositional variations.

using ASTER's SWIR bands for mineral (group) mapping have been noted due to the crosstalk issue where stray light from band 4 'leaks' as an additive noise signal into bands 5 and 9 (Iwasaki *et al.* 2001). An algorithm and software fix were developed and applied to correct for this miscalibration issue (Iwasaki & Tonooka 2005); however, in areas of low ground reflectance (*e.g.* shadow, thick vegetation, dark surfaces) a residual crosstalk effect is apparent and can lead to 'false anomalies' using spectral band indices (Hewson *et al.* 2005; Hewson & Cudahy 2011). A recent review of multi- and hyperspectral remote sensing techniques considered ASTER's crosstalk issue as making interpretation of band absorptions 'not feasible' (van der Meer *et al.* 2012). However, Mars and Rowan (2010) contend that *in situ* or spectral reference calibration within study areas can overcome such errors within ASTER's SWIR bands.

Early ASTER case studies also showed the usefulness of integrating processed ASTER map products with airborne geophysics such as radiometrics (Hewson *et al.* 2003a). In particular, sericite/mica can be discriminated within ASTER map products generated for the AlOH mineral group using potassium radiometrics at Broken Hill (Hewson *et al.* 2003a). Integrating Landsat TM (Ricchetti 2000) and ASTER imagery (Hewson *et al.* 2006) with Digital Elevation Model (DEM) information has also improved the classification and interpretation of the geomorphology and geology. In particular ASTER interpreted quartz mineral occurrences related to transported sandy alluvial cover can be easily discriminated from silicified rock outcrops with slope and shaded DEM products (Hewson *et al.* 2006).

CSIRO-GA Australian ASTER geoscience map products

The Australian ASTER products released by CSIRO and GA provided the first continent-wide mosaic of satellite-derived mineral mapping (Cudahy 2012; Caccetta *et al.* 2013). Prior to the generation of such Australian continental-scale compositional maps, isolated and independent industry and government agency projects provided useful, albeit sometimes haphazard, application of

Downloaded by [RMIT University] at 15:23 18 February 2015

Downloaded by [RMIT University] at 15:23 18 February 2015

ASTER for limited Australian areas using a variety of methodologies and reference standards. The Mosaics of thousands of Australian ASTER radiance scenes were calibrated using many hyperspectral satellite reflectance reference surveys in conjunction with illumination and atmosphere-based gain and offset corrections (Cudahy 2012; Caccetta *et al.* 2013). This calibration of ASTER imagery using multiple reflectance reference areas attempted to reduce the effects of crosstalk, variable illumination and ground cover conditions (Caccetta *et al.* 2013). Subsequent processing into band (ratio) parameters, targeting composition-related spectral absorption features, provided a generally reliable approach for generating map products across Australia (Cudahy 2012; Caccetta *et al.* 2013). The values produced by these band parameter ratio products provided a unit-less and relative estimate of abundance or indicator of composition depending on the nature of the described product. Masking of resulting band parameter products was performed to exclude areas of cloud cover, deep shadow, water bodies and significant vegetation followed by the application of consistent thresholds that best qualitatively to semi-quantitatively represented mineral (group) surface content and likely mineral species composition of rock/soil exposures. Since the launch of the CSIRO-GA Australian ASTER Geoscience Map products, Laukamp *et al.* (2013) recently demonstrated their application for mineral exploration in the Jervois Block arid environment of central Northern Territory. Table 2 summarises the 17 ASTER products and their inferred accuracies (Cudahy 2012).

A comprehensive description of Australian ASTER Geoscience Map products is presented by Geoscience Australia (http://www.ga.gov.au/earth-observation/satellites-and-sensors/aster-radiometer/national-aster-maps.html). Also NASA-developed World Wind software (http://www.ga.gov.au/aster-viewer) has been promoted as a user-friendly method of visualising these CSIRO-GA Australian ASTER geoscience map products in conjunction with topographic information and other geophysical datasets such as radiometric data (Figure 5). Figure 5 shows an example of this web-based software and locations of the Wagga Wagga and Mt Fitton test sites used in this study, overlain with the ASTER false-colour map product. These ASTER map products in GeoTIFF file format can be accessed from the AuScope Discovery Portal (http://portal.auscope.org/portal/gmap.html) or CSIRO's site C3DMM (http://c3dmm.csiro.au). In this study, the ASTER map products in binary sequential (BSQ) format were also used to examine the effects of different histogram stretches applied to a variety of band ratio imagery.

2. Test site areas – environment and geology

Wagga Wagga, NSW

The area of the Wagga Wagga 1:100 000 (100 K) map sheet of south eastern NSW was examined in this study and encompasses regolith and landforms typical of the Riverine Plains adjacent to the Murrumbidgee River (Figure 6). In particular, it has elevations ranging from 180 m to above 500 m, experiencing a moderate rainfall between 500 mm and 650 mm per annum (Chen 1997). The majority of the map sheet area is actively farmed, either as crops or under sheep or cattle grazing. Landforms consist of floodplains to moderately hilly areas with some eroded plateau exposures and piedmonts (Chen & McKane 1997). Chen (1997) described and analysed the geomorphology and landforms, in part using slope percent (%) estimates of the various floodplains and tributaries (1–2 percent), undulating plains and rises (3–5 percent), and hilly areas vulnerable to erosion (10–30 percent). Surface soils typically include clay-rich alluvial and gravels with a strong presence of aeolian ('parna') sediments, particularly blanketing areas of lower relief. Extensively folded Ordovician metasediments, large

Table 2. Summary of the 17 CSIRO-geoscience ASTER compositional map products (Cudahy 2012)

Product name (product spatial resolution)	Surface composition/Example minerals targeted	Accuracy
1. False colour (30 m)	Standard VNIR product, green vegetation highlighted in red	N/A
2. Landsat TM Regolith Ratios (30 m)	Green vegetation **versus** different geological/regolith areas	N/A
3. Green vegetation Content (30 m)	Green vegetation	Moderate
4. Ferric oxide content (30 m)	Hematite, goethite, jarosite	Moderate
5. Ferric oxide composition (30 m)	Hematite **versus** goethite	Moderate
6. Ferrous iron index (30 m)	As incorporated within silicates/carbonate	Moderate
7. Opaque index (30 m)	Includes carbon black (e.g. ash), magnetite, Mn oxides, and	Moderate
8. AlOH group content (30 m)	Phengite, muscovite, paragonite, illite, montmorillonite, kaolinite	Moderate
9. AlOH group composition (30 m)	Ordered kaolinite, Al-rich white mica (*e.g.* muscovite, paragonite) **versus** Al-poor (also Si- or K-rich) white mica (*e.g.* phengite)	Moderate
10. Kaolin group index (30 m)	Pyrophyllite, alunite, well-ordered kaolinite	Moderate
11. FeOH group content (30 m)	Chlorite, epidote, jarosite, gibbsite, gypsum,	Low
12. MgOH group content (30 m)	Calcite, dolomite, magnesite, chlorite, amphibole, talc.	Moderate
13. MgOH group composition (30)	Dolomite, amphibole, chlorite **versus** Calcite, amphibole.	Moderate
14. Ferrous iron content in MgOH/ carbonate (30 m)	Low ferrous iron carbonate/MgOH minerals (*e.g.* talc) **versus** High ferrous iron carbonate/MgOH minerals (*e.g.* chlorite).	Moderate
15. Silica index (90 m)	SiO_2 content, quartz content enhanced by grain texture	Moderate
16. Quartz index (90 m)	Quartz	Low
17. Gypsum index (90 m)	Gypsum	Very Low

Downloaded by [RMIT University] at 15:23 18 February 2015

intrusive Silurian granite bodies, and minor Devonian sandstones occupy hilly areas, mostly encompassing the eastern and south eastern parts of the Wagga Wagga 100 K map sheet area (Raymond 1993).

The proximity of the Wagga study area to the Gilmore Fault and the Gidginbung/Adelong gold deposits provided possible models and references in the search for prospective targets (Downes *et al.* 2004; Lewis & Downes 2008). Studies of the Lachlan orogenic gold deposits, including the Adelong deposit, generally show an alteration assemblage that includes sericite, muscovite–phengite and/or carbonates (Downes & Seccombe 2008), and they are potentially mapped by the AlOH and MgOH/carbonate ASTER map products. The alteration at the Gidginbung deposit consists of several zones that include silica/quartz, kaolinite and illite (Downes *et al.* 2004) – also potentially mappable by the ASTER AlOH and silica index/quartz products. As a result, one of the aims in the study of the Wagga Wagga test site is to observe the ability of the ASTER map products to discriminate such AlOH (e.g. sericite/white mica), MgOH/carbonate and silica/quartz contents.

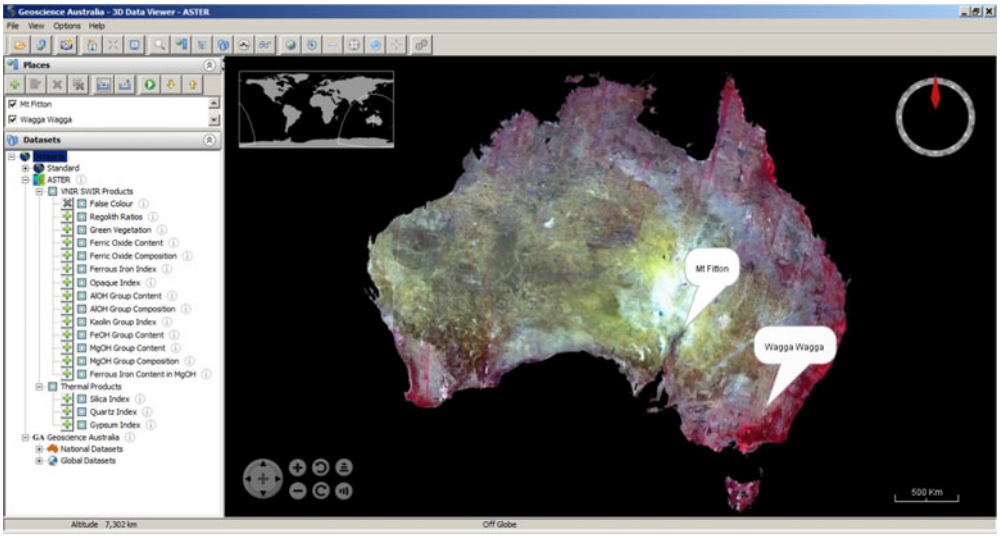


Figure 5. Example of the Geoscience Australia ASTER World Wind website highlighting locations of Wagga Wagga and Mt Fitton test sites overlain on ASTER false-colour product (http://www.ga.gov.au/aster-viewer).

Mt Fitton, SA

The Mount Fitton area (139°25′E, 29°55′S) in the northern Flinders Ranges, 600 km north-northeast of Adelaide, South Australia, has a semi-arid climate which receives less than 250 mm rainfall per year. Generally, the vegetation is sparse, ranging between 5 and 15 percent total cover. Regional topography provides a relief of up to 1000 m, but Mt Fitton's localized relief is generally only 100 m. Flash flooding has stripped unconsolidated regolith material, leaving abundant fresh exposures of bedrock. Mt Fitton contains a variety of intrusive and sedimentary units, with some greenschist metamorphic and localized hydrothermal alteration. Geological mapping by Coats and Blissett (1971) found Precambrian granites, amphibolite dykes, and tightly folded and faulted tillites, siltstones and carbonates. Precambrian Terrapinna Granite basement rocks are exposed in the northeast part of the study area (Figure 7). This area is overlain by the Umberatana Group, which includes the quartz-rich Mount Curtis Tillite and Bolla Bollana Formation. The published maps identify zones of alteration and mineralisation, such as the greenschist facies and dolomite/magnesite development within the Balcanoona Formation. Localised hydrothermal alteration has resulted in the formation of talc, tremolite, chlorite, scapolite, muscovite, and/or quartz in the carbonate sequences. Talc has been mined from the area including the Mt Fitton Talc Mine (Figure 7). Alteration and mineralisation has also been associated with the Mt Fitton Anticline striking in an east-west direction through the centre of the test site (Figure 7) (Sheard 2012).

The Mt Fitton area has previously been extensively used as a test site for both airborne and satellite-borne remote sensing (Hewson *et al.* 2003b). In particular Mt Fitton was used for an early demonstration of ASTER mapping capabilities (Hewson *et al.* 2001). A study of ASTER sensor issues for geological mapping was also undertaken at Mt Fitton using a comparison with airborne hyperspectral (HyMap) imagery (Hewson & Cudahy 2011).

Downloaded by [RMIT University] at 15:23 18 February 2015

Downloaded by [RMIT University] at 15:23 18 February 2015

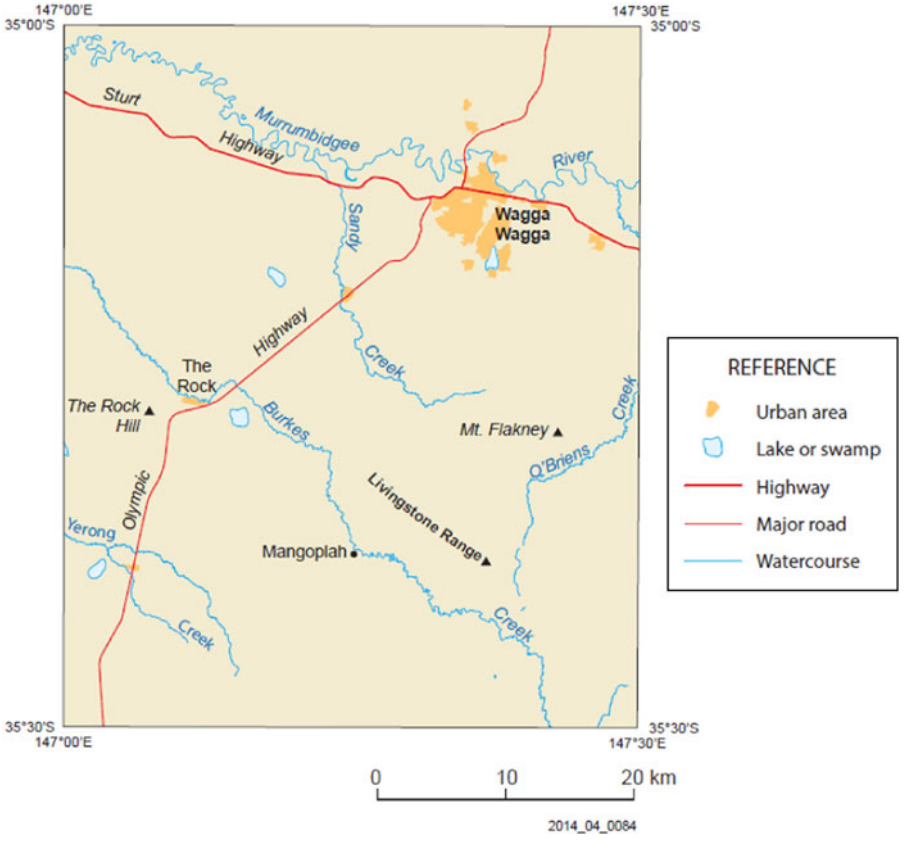


Figure 6. Location and watercourses within the Wagga Wagga 100 K map sheet (Hewson & Robson 2014).

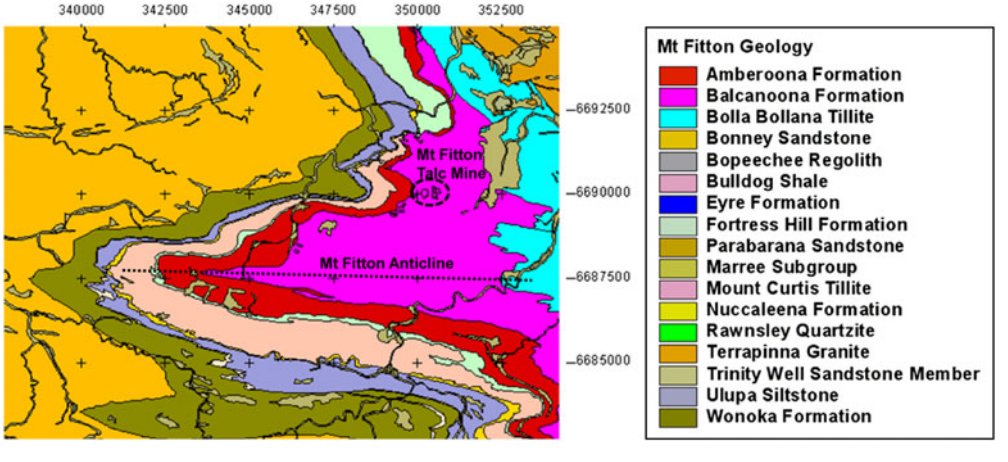


Figure 7. Mt Fitton geological map (Coats & Blissett 1971).

Downloaded by [RMIT University] at 15:23 18 February 2015

3. Datasets and methodologies

ASTER

GeoTIFF and BSQ binary-format versions of the ASTER map products were utilised in this study, as made available by CSIRO and Geoscience Australia via the GSNSW. The 17 ASTER products (Table 2) were visualised with ENVI™ (http://www.exelisvis.com), ERMapper™ (http://geospatial.intergraph.com/Homepage.aspx) and Global Mapper™ (http://www.bluemarblegeo.com/products/global-mapper.php) software where map sheet boundaries, drainage and other relevant topographic Geographic Information System (GIS) shapefile information were incorporated. ERMapper™ and Global Mapper™ proved the most user-friendly software when integrating with geophysical and other data sets of different dimensions and origins. BSQ-format versions of the ASTER map products were useful when examining variations of the imagery and generated mineral anomalies applying different image histogram stretch methods.

The ASTER acquisition dates of imagery used for the generation of mineral map products in the Wagga Wagga and Mt Fitton study areas were determined by examining the ASTER archive listed within the United States Geological Survey (USGS) Glovis site (https://lpdaac.usgs.gov/data_access/glovis). The major portions of the Wagga Wagga 100 K map sheet and the Mt Fitton area were acquired with ASTER on 11 January 2001 and 11 April 2001, respectively.

Geo-location registration of the CSIRO/Geoscience Australia ASTER map products was provided by the original ASTER L1B imagery (Caccetta *et al.* 2013). The spatial accuracy of the ASTER L1B product has been estimated as better than 50 m (Iwasaki and Fujisada 2005), with some reported accuracies for scenes over flat relief well below this figure (20–30 m) (Watanabe 2005). This was considered sufficient for typical mineral exploration and integration with the spatial information applied here.

Airborne geophysics

Various radiometric and filtered total magnetic intensity (TMI) or aeromagnetics data sets, processed into 50 m grids, were obtained by the GSNSW for the Wagga Wagga 100 K map sheet. High-frequency filtered aeromagnetic data such as Tilt angle filtered TMI and first vertical derivative (1VD) TMI were also examined for near-surface magnetic anomalies relevant for comparison with the near-surface sensing radiometrics and ASTER. Radioelements potassium (K), thorium (Th) and uranium (U) and the ternary RGB composite imagery (e.g. red, K; green, Th; blue, U) were useful to compare with surface remote sensing compositional imagery although they typically sense deeper into the subsurface (up to ~30 cm). Airborne radiometrics and TMI data, processed as 100 m grids, were also used for the Mt Fitton area as obtained by the Geological Survey of South Australia (GSSA).

Digital elevation models (DEMs)

DEMs were available from the GSNSW, GSSA and also from the Shuttle Radar Topography Mission (SRTM) at 80 m x-y spatial resolution (http://www2.jpl.nasa.gov/srtm/). ENVI™ was used to process DEM data into topographic models that included slope percent, aspect and artificial sun shaded relief imagery. Figure 8a displays the SRTM 80 m slope for relief greater than 10 percent combined with classified landscapes by Chen (1997), highlighting the steeper slopes that occur within Chen's divisions IV and V. Thresholded slope percent imagery derived from the Wagga Wagga 100 K SRTM DEM data was used to extract ('mask') only areas greater than 10 percent in order to focus on potentially hilly and piedmont rock/talus outcrop exposures within the combined ASTER-geophysics products.

AusCover fractional landcover

Australia's land surface has been recently analysed for fractional cover percentages of

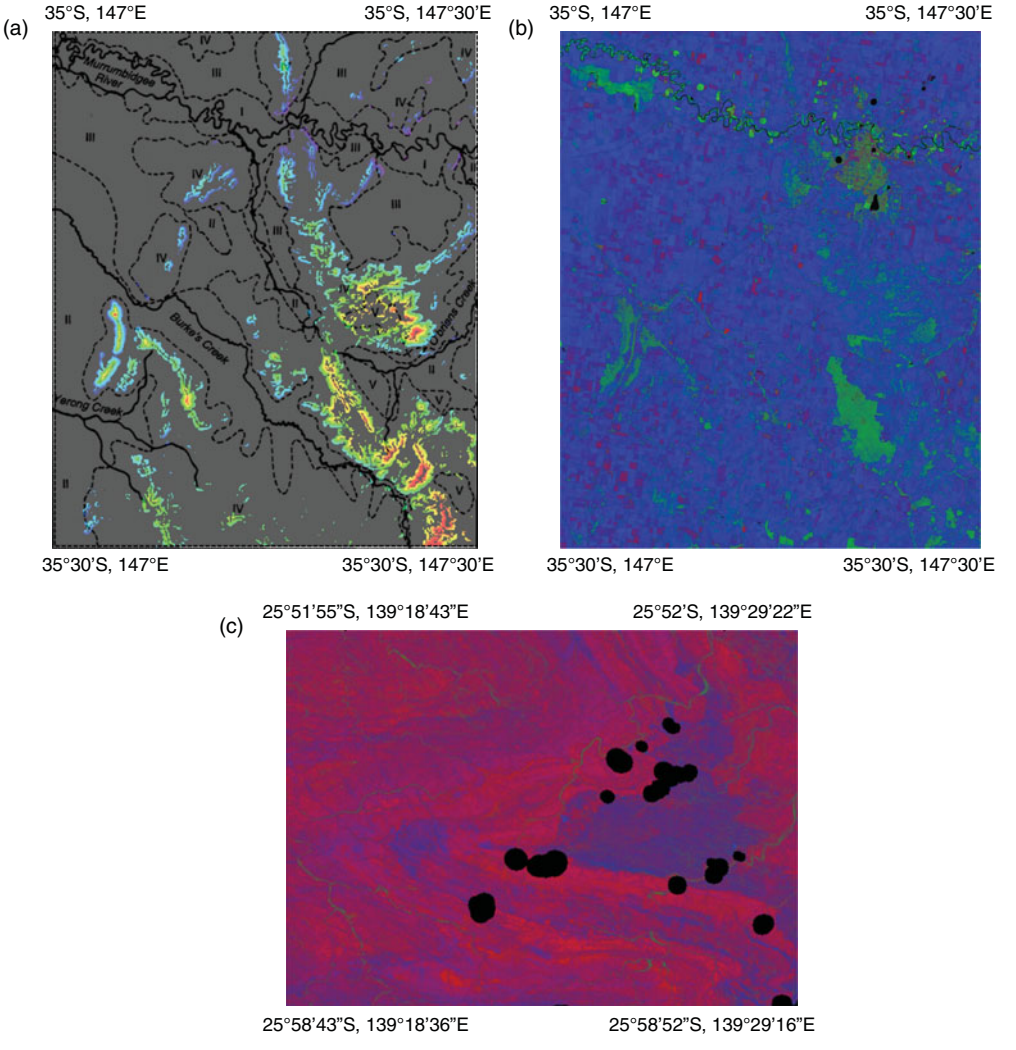


Figure 8. (a) Wagga Wagga 100 K landscape divisions overlying SRTM 80 m DEM slopes greater than 10 percent where blue = 150 to red = 300 m elevation. Landscape divisions: (I) Murrumbidgee floodplains; (II) alluvial plains of local streams; (III) undulating plains, rises, and long footslopes; (IV) hilly areas; and (V) eroded plateau and piedmont plains (Chen 1997); (b) Wagga 100 K Landsat 7-derived fractional cover RGB image: red, bare ground; green, photosynthetic vegetation; blue, non-photosynthetic vegetation (linear stretch, 0–100 percent); (c) Mt Fitton area Landsat 7-derived fractional cover RGB image. Red, bare ground; green, photosynthetic vegetation; blue, non-photosynthetic vegetation (linear stretch, 0–100 percent). Masking of unresolved fractional areas shown in black.

bare ground (*e.g.* soil, rock outcrop), green vegetation and dry vegetation cover as part of the Terrestrial Ecosystem Research Network (TERN; http://www.tern.org.au/). Datasets are available as part of this project via the AusCover data facility (http://data.auscover.org.au/). In this study, the AusCover processed Landsat TM 5 and 7 derived fractional cover analysis provided the 30 m spatial resolution for the Wagga Wagga and Mt Fitton study

Downloaded by [RMIT University] at 15:23 18 February 2015

areas. This coverage information was generated by algorithms described by Scarth *et al.* (2010) and available via AusCover as binary NetCDF data tiles (http://data.auscover.org.au/xwiki/bin/view/Product+pages/Landsat+Fractional+Cover#HLinktothedata). The Landsat 7 derived cover information were generated from the imagery recorded on 10 January 2001, the previous day of the Wagga Wagga ASTER acquisition. The closest Mt Fitton Landsat 5 (or 7) imagery to the ASTER acquisition (11 April 2001) was on 20 October 2001; however, comparisons of the ASTER green vegetation and Landsat 7 derived cover imagery over Mt Fitton did not reveal significant differences. Figures 8b and 8c display the fractional cover product as a RGB composite for bare ground, green and dry vegetation for the Wagga Wagga 100 K map sheet and the Mt Fitton areas, respectively. In this study, masks based on the photosynthetic vegetation fraction for values less than 45 percent to refine (i.e. filter) were applied on some of the final Wagga Wagga ASTER map examples. This was found unnecessary for the Mt Fitton ASTER products due to the abundance of bare ground (red areas, Figure 8c) and lack of photosynthetic vegetation (green, Figure 8c).

Field studies and sample spectroscopy

Field sampling and validation of identified ASTER mineral map anomalies were undertaken in the Wagga Wagga area during April 2013 in the form of observed waypoints and as sampling localities. A total of 69 total observed localities ('WPxx', Figure 9) with 29 of them sampled for rocks/soil were undertaken. These observed and sampled localities were chosen for their anomalous ASTER mineral map occurrences, or as representative examples of various soil and geological units. All collected field samples

Downloaded by [RMIT University] at 15:23 18 February 2015

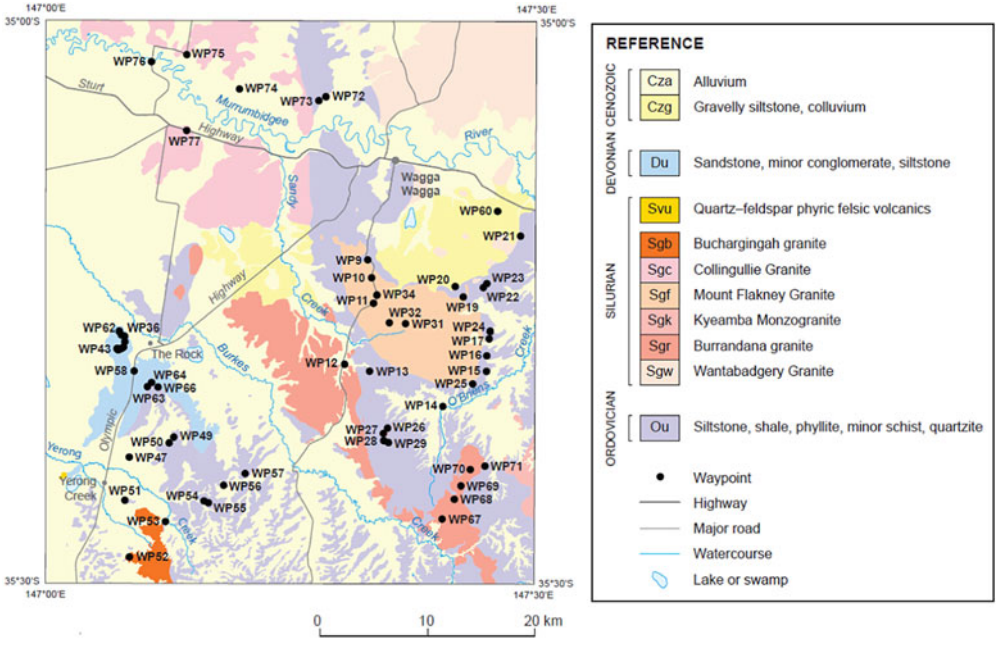


Figure 9. Wagga Wagga 100 K map sheet geology (Raymond 1993) and the observed localities (WPxx) (Hewson & Robson 2014).

Downloaded by [RMIT University] at 15:23 18 February 2015

were measured with ASD's Terraspec 4 VNIR-SWIR spectrometer (http://www.asdi.com/products/terraspec/terraspec-hi-res-mineral-spectrometer). A complete description of spectral measurements within the Wagga Wagga 100 K area and their interpretation is available in Hewson (2013). Previous comparisons between the measured reflectance signatures of Mt Fitton field rock/soil samples and ASTER or HyMap signatures are described in Hewson *et al.* (2001) and Hewson and Cudahy (2011).

4. Results

Mt Fitton test site

The Mt Fitton ASTER image utilized for the GA-CSIRO ASTER map products appeared to be acquired under optimal illumination conditions with minimal vegetation cover and cloud-free conditions (Figure 10a). Some topographic relief was apparent; however, no deep shadows were apparent. The ASTER AlOH group content highlights an area of sericite mica alteration at the nose of the Mt Fitton Anticline, particularly within the Amberoona Formation (Figure 10b). The Balcanoona Formation (Figure 7), consisting predominantly of the carbonate mineral dolomite, was highlighted by the ASTER MgOH group content product (green to yellow areas, Figure 10c). Although dolomite is a carbonate mineral and not of the MgOH mineral group, the overlap of their SWIR diagnostic signatures and the moderate spectral resolution of the ASTER bands precludes a specific abundance index for dolomite alone (Table 2 outlines the minerals potentially discriminated from each ASTER map product; Cudahy 2012). The ASTER MgOH composition index (Figure 10d) appeared successful in discriminating some of the replacement mineralised talc and chlorite occurrences within the Balcanoona dolomite. A Red

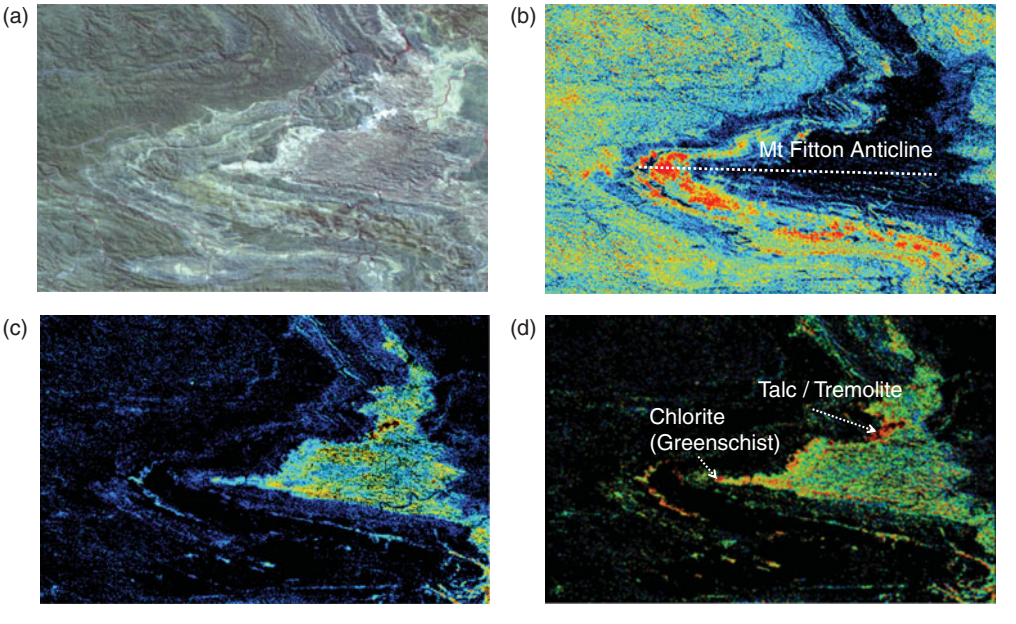


Figure 10. Mt Fitton ASTER map products: (a) ASTER false colour; (b) AlOH group content; (c) MgOH (and carbonate) group content; (d) MgOH (and carbonate) group composition. The extents and location of this image correspond to Figures 7 and 8c.

Green Blue (RGB) composite image of the ASTER products AlOH group (red), ferric Iron oxide (green) and silica (blue) demonstrates the ASTER mapping's ability to discriminate many of the lithological units shown within the published geology (Figure 7) as well as potential areas of alteration including sericitisation (Figure 11a,b). Subtle variations within such RGB composite imagery appear to offer a potential to further subdivide the mapped stratigraphic units. For example, the Bonney Sandstone (Figure 7) in the north-western portion of the Mt Fitton area shown appears to contain units of variable clay and ferric iron content (Figure 11b). Although the RGB composite imagery was designed using the thresholds recommended by Cudahy (2012) for each of the individual mineral products, care is required in the interpretation of the combined three products. For example, the low abundance of two minerals potentially visually exaggerates the third mineral product.

Airborne geophysics for the Mt Fitton area highlighted chemistry and physical variations rather than mineralogy alone. In particular the radiometrics products of potassium (K), thorium (Th) and uranium (U) discriminated some of the Mt Fitton units (Figure 11c) such as the Balcanoona Formation with low K, Th and U but showed a broader chemical overlap across the stratigraphy. Several units from the Wonoka to the Amberoona Formations displayed a K-bearing chemistry, possibly associated with a clay or chlorite bearing mineralogy (Figure 11c). The aeromagnetic TMI data was processed into 1VD with the aim of highlighting near-surface magnetic (possibly magnetite mineral associated) anomalies and structural features (Figure 11d). A high 1VD anomalous response occurred along the nose

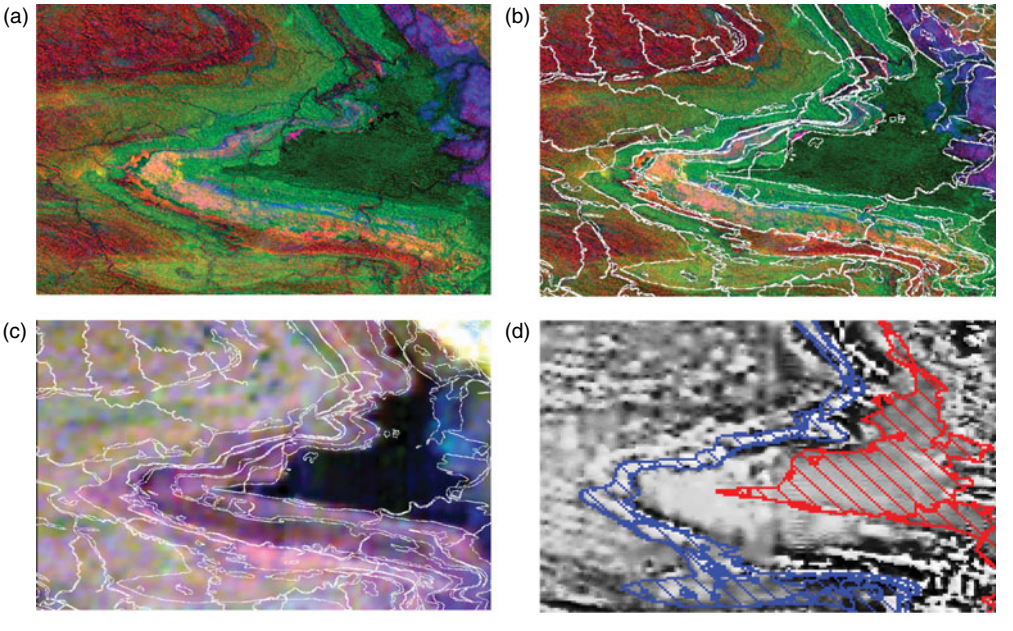


Figure 11. Mt Fitton integrated imagery. (a) ASTER RGB composite: red, AlOH group content; green, ferric iron oxide; blue, silica index; (b) ASTER RGB composite (a) with Mt Fitton published geology overlay (Coats & Blissett,1971); (c) Radiometrics RGB composite: red, K; green, Th; blue, U; with Mt Fitton published geology overlay (Coats & Blissett,1971); (d) Greyscale image of 1VD TMI with Balcanoona (red) and Wonoka (blue) Formations (Coats & Blissett,1971). The extents and location of this image correspond to Figures 7 and 8c.

Downloaded by [RMIT University] at 15:23 18 February 2015

of the Mt Fitton Anticline between the Balcanoona and Wonoka Formations (Figure 11d).

An examination of the possible relationship between the radiometric K and ASTER AlOH composition was attempted using ENVI's two-dimensional (2D) scatterplot function to test possible potassium-bearing clay associations (Figure 12a, c). The scatterplots indicated that there was no coherent relationship or correlation (Figure 12a,c). Density-slicing the radiometrics potassium and ASTER AlOH composition data, however, indicated some interesting differences between the two techniques. Higher AlOH group composition index values associated with Al-poor mica chemistry ('phengite') were apparent along the Mt Fitton Anticline and units folded around the Balcanoona Formation and distinct from the Bonney Formation micas (yellow, Figure 12b). The published Mt Fitton geology is shown as a black and white background (Figure 12b,d) based on Figure 7. A four-density-slice classification of the potassium data discriminated several units, including the tillites (green, Figure 12d; Mt Curtis and Bolla Bollana Formations), the Balcanoona dolomite (blue, Figure 12d) and the Terrapina Granite (yellow, Figure 12d). It appears that the ASTER AlOH composition product highlights variations in mica chemistry, related to structurally active versus inactive areas, whilst the radiometric potassium highlights broader changes in host rock mica (and feldspar) chemistry.

Wagga Wagga 100 K map sheet

The Australian ASTER GeoTIFF map products were initially examined individually for the Wagga Wagga 100 K map sheet. Several of

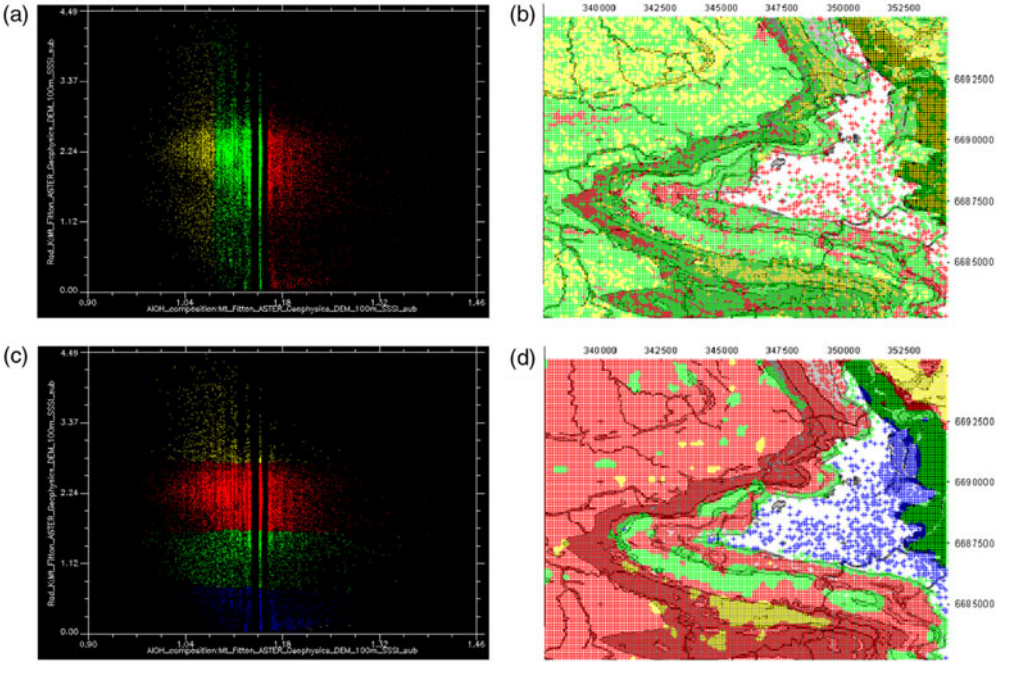


Figure 12. (a) 2D scatter plot of radiometric K versus ASTER AlOH group composition (as three density slices); (b) corresponding Mt Fitton classification from (a) over published geology; (c) 2D scatter plot of radiometric K (as four density slices) versus ASTER AlOH group composition; (d) corresponding Mt Fitton classification from (c) over published geology. Note the classification colours shown in (b) and (d) correspond to the regions of interest marking the density slices of the 2D scatterplots (a) and (c), respectively.

Downloaded by [RMIT University] at 15:23 18 February 2015

the 17 products did not show significant anomalies related to geological features and were limited to cultivated cropping patterns at best. In particular the ASTER imagery used here was acquired in mid-summer 2001 and highlighted exposed fallow fields and soils (Figure 13). The ASTER false-colour map product (Figure 13) also highlighted the town of Wagga Wagga and several vegetated areas with topographic relief (dark red to dark grey). A slight boundary anomaly is apparent at the far north-western portion of the 100 K scene from a change of ASTER scenes.

ASTER's green vegetation product (Figure 14a) corresponds approximately with areas of red shown in the ASTER false-colour product (Figure 13) although it is more correctly generated by a band ratio (band 3/band 2) targeting the chlorophyll 'red edge'. Exposed soil and fallow crop fields have no or low green vegetation anomalies (blue) on the floodplains and lowlands while vegetation is highlighted in areas of topographic relief (Figures 8a,b, 13, 14a). ASTER's AlOH group content product (Figure 14b) shows limited clay anomalies except for the Wagga

Downloaded by [RMIT University] at 15:23 18 February 2015

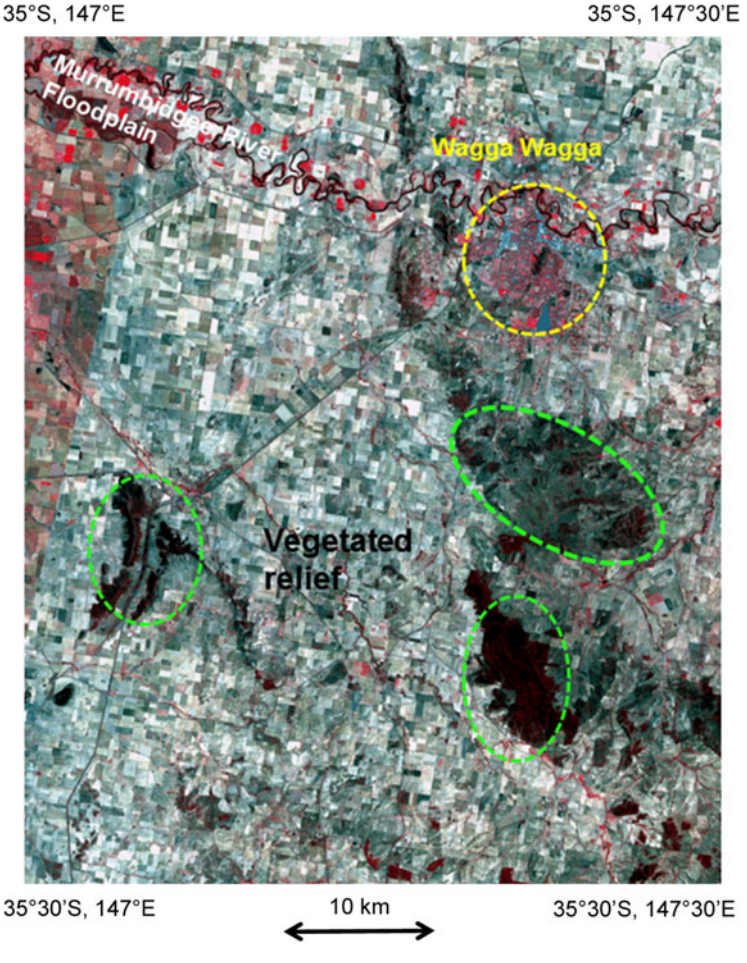


Figure 13. ASTER false-colour product within the Wagga Wagga 100 K map sheet. Areas of relief with vegetation are highlighted by green dashes.

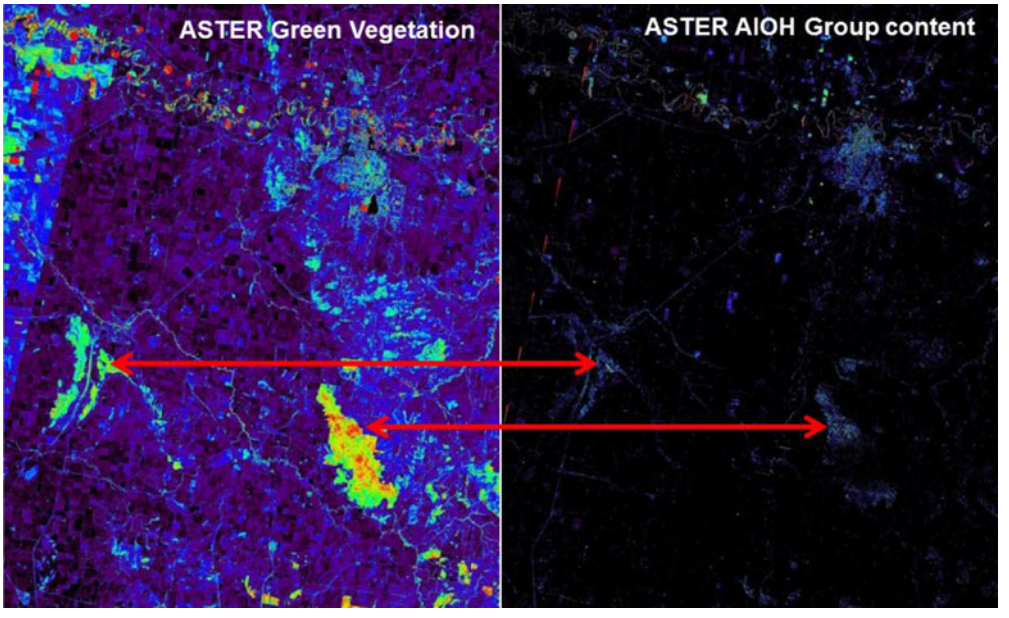


Figure 14. (a) Wagga Wagga 100 K ASTER green vegetation product (blue, low; red, high content); (a) ASTER AlOH content (blue, low; red, high content).

Downloaded by [RMIT University] at 15:23 18 February 2015

Wagga township and an apparent association with vegetated anomalies shown in the green vegetation product (Figure 14a). A green vegetation mask, based on the ASTER product, was applied during the generation of the AlOH group composition map product (Cudahy 2012) and minimal anomalies were apparent.

ASTER's ferric oxide content product (Figure 15) showed elevated values in comparison with the AlOH group content (Figure 14b). Some linear trends were apparent although the anomalies were often biased by the cropping patterns and exposed paddock soils. Nonetheless some linear trends highlighted (red dashed lines) boundaries and possible lineaments related to either floodplain alluvium, regolith or geological units. Although Cudahy (2012) describes the ferric oxide content as having moderate accuracy, a comment is also noted for the potential of mixing errors and an inverse relationship with the green vegetation product. This could also be related either to the obscuring effect of vegetation/crops, or spectral signature ambiguities given the proximity of VNIR spectral features. The ASTER FeOH and ferrous iron products in the Wagga Wagga 100 K area did not generate coherent or distinct features apart from some isolated paddock anomalies. These products as well as the MgOH group content, MgOH group composition and kaolin group index products also had a green vegetation mask applied, based on the corresponding ASTER product (Cudahy 2012).

The nature of the geomorphology and presence of extensive agricultural cultivation within the Wagga Wagga 100 K map sheet prompted the use of DEM data to discriminate the likely geologically exposed areas as suggested by Chen (1997) in higher slope relief areas of landscape divisions of (IV) and (V). Processing the SRTM 80 m DEM for slope percent (%) information enabled the generation of a mask based on slopes greater than 10 percent to apply to the ASTER map

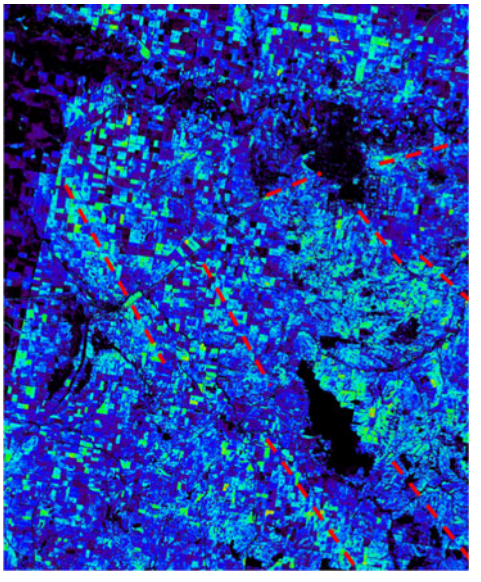


Figure 15. Wagga Wagga 100 K ASTER ferric oxide content. Apparent trends in the ferric oxide content are shown in red dashed lines.

products and enhance the likely mineral spectral anomalies associated with rock outcrops.

The ASTER silica index highlighted some anomalies, although the range in values was limited. Such anomalies occurred within paddocks, and also as broader subtle variations in higher-relief areas. An attempt to overcome the observed limited range of the silica index values was undertaken using a histogram equalisation data stretch, still within the thresholds advised by Cudahy (2012) (Figure 16a). The result highlighted both more noise and some coherent spatial anomalies (Figure 16a). Masking of this product with SRTM 80 m slope product greater than 10 percent (Figure 16b) enhanced interpretation of the coherent silica/quartz-rich anomalies, exclusive of the generally lower-relief cropland (Figure 16b). Elevated areas of the quartz-rich sandstone outcropping Bulloc Ranges and metasedimentary outcropping Livingstone Ranges were highlighted by this approach (Figure 16b).

A similar approach to displaying and enhancing the Wagga Wagga 100 K ASTER map products was applied to the airborne radiometrics where anomalous regions were

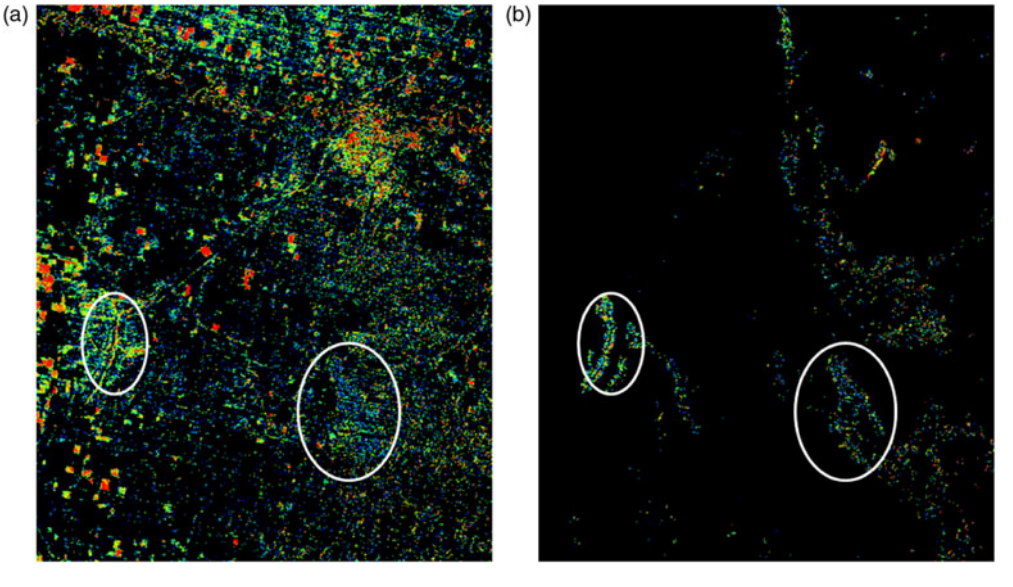


Figure 16. (a) Wagga Wagga 100 K ASTER Silica Index product generated with a histogram equalisation stretch; (b) histogram equalised ASTER silica index masked for slope > 10 percent. Areas highlighted (white) show the Bulloc Ranges and the Livingstone Ranges within the western and eastern portions of the map sheet respectively.

Downloaded by [RMIT University] at 15:23 18 February 2015

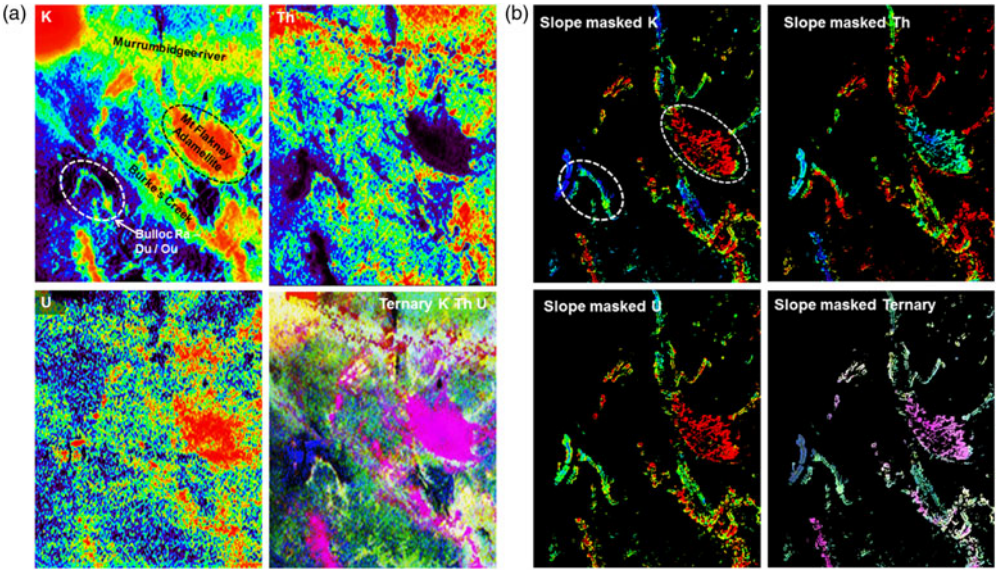


Figure 17. (a) Wagga Wagga 100 K airborne radiometrics, K, Th, U and as a ternary imagery (RGB: K, Th, U), displayed with a histogram equalization stretch; (b) K, Th, U and ternary imagery (RGB: K, Th, U), masked for slopes >10 percent, displayed with a 2 percent linear histogram stretch.

extracted within the areas of elevated slope. Histogram equalisation stretching of the K, Th and U radioelements highlighted a mixture of alluvial deposition and outcropping geology (Figure 17a). The potassium radiometrics coherently mapped the alluvium and floodplains of Burke's Creek and Murrumbidgee River (Figure 17a). The Mount Flakney Adamellite and the Bulloc Ranges Ordovician (Ou) and Devonian sandstones (Du) were highlighted as anomalous using the entire 100 K map sheet data set (with histogram equalisation) but more subtle variations in radioelement composition were apparent when slope masking was applied and simple 2 percent linear used for image stretching (Figure 17b). Mapping the compositional variations within these units appeared to be enhanced by focussing to areas of higher relief. For example, K, Th and U radiometric variations within the Bulloc Ranges Du/Ou units are discriminated more clearly (Figure 17b). Increased thicknesses of aeolian, alluvium or colluvium deposits on lowlands and areas of reduced slope may mask and dilute radiometric sensing of some of the geological units of interest.

Filtered aeromagnetic data for the Wagga Wagga 100 K map sheet was applied to extract structural information and also to highlight near-surface trends of iron-bearing units/magnetite and possible correlations with the ASTER map products. ASTER's ferric oxide content showed some trends, albeit revealed within exposed paddocks (Figure 15), that showed NW and some possible NE trending features that correlated approximately with Tilt filtered TMI lineaments (Figure 18). The VNIR spectral signature of magnetite is essentially aspectral and not likely to be revealed by the ASTER ferric oxide content product directly. However, the presence of underlying magnetite-bearing rocks may possibly be associated with increased ferric iron oxide content.

A combined ASTER-geophysics interpretation was undertaken within The Rock Hill (35°16′54″S, 147°5′5″E) and Flowerpot Hill (35°17′55″S, 147°6′4″E) of the Bulloc Ranges

Downloaded by [RMIT University] at 15:23 18 February 2015

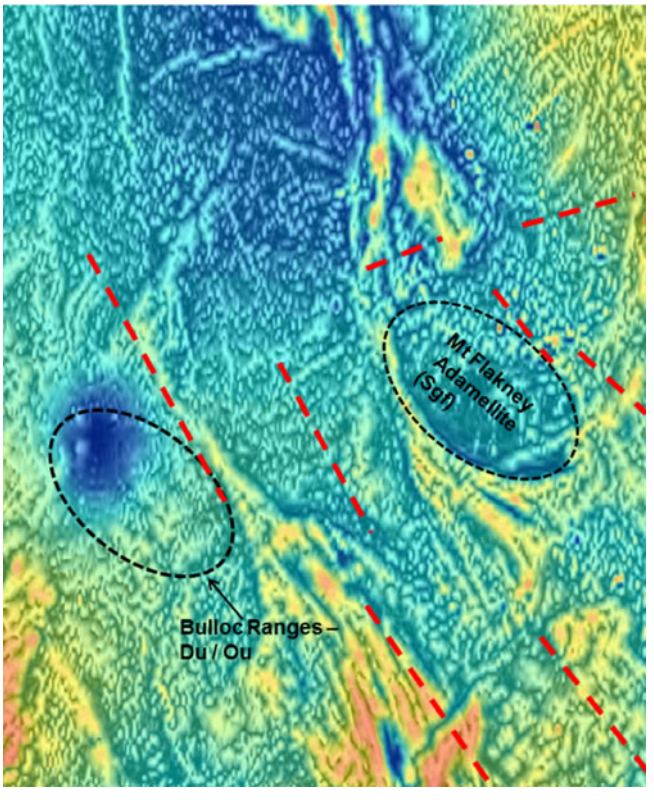


Figure 18. Pseudo-colour displayed TMI draped over Tilt filtered TMI data (greyscale). Apparent trends in the ASTER ferric oxide content (Figure 15) are shown as red dashed lines. The relationship of features to the Bulloc Ranges metasediments (Du/Ou) and the Mt Flakney Adamellite (Sgf) is shown.

(Figure 18) (Hewson 2013; Hewson & Robson 2014). The silica index and the AlOH group content map products, masked for green vegetation and high slopes, appeared to highlight anomalous values along a structural fold axis that had associated radiometric K overprinting, a pronounced magnetic low and interpreted lineament, suggestive of an alteration setting. Field observations indicated increased quartz presence and rock sample spectral signatures exhibiting hematite and the AlOH mineral phengite.

ASTER data interpretation issues

Acquisition of ASTER satellite imagery at approximately 10:30 am can potentially produce sharp shadows on steep westerly slopes within high-relief areas. The ASTER satellite sensor has an additional issue of potential false anomalies from the crosstalk mis-calibration of its shortwave IR sensor (bands 5–9), as used for the generation of AlOH group content or composition mineral maps. Dark shaded areas appear on the western slopes of The Rock Hill and Flowerpot Hill as a result of north and north-west trending ridges, as shown in the sun shaded DEM imagery generated to simulate illumination conditions on 11 January 2001 at 10:30 am (blue ellipses, Figure 19a). These areas of deep shadow appear to be coincident with some of the ALOH group content anomalies (blue ellipses, Figure 19b) and potentially the result of false anomalies associated with crosstalk. However, areas of full illumination on the

Downloaded by [RMIT University] at 15:23 18 February 2015

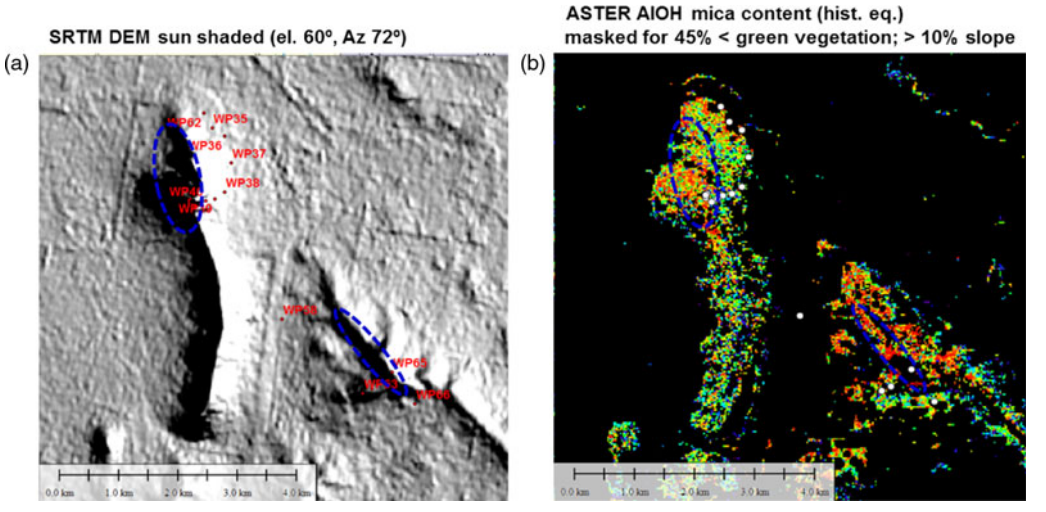


Figure 19. (a) Sun shaded SRTM 80 m DEM of The Rock and Flowerpot Hill (60° elevation, 72° azimuth) simulating illumination conditions and shaded relief during ASTER image acquisition (11 January 2001); (b) ASTER AlOH group content and corresponding areas of shaded relief (blue ellipses).

north-east slopes also show AlOH anomalies and the crosstalk explanation does not entirely negate the AlOH presence. These anomalous areas are potentially exaggerated by the use of histogram equalised data stretching; however, this effect also appears apparent within the dark vegetated areas discussed for Figure 14a, b, assuming linear stretching. These issues are discussed in greater detail for ASD spectrally measured asphalt reference sites at Wagga Wagga (Hewson 2013; Hewson & Robson 2014).

Field observations and ASD *in situ* field measurements of gravel lag, vegetation, ground litter etc., Waypoint WP62 (Figures 9a, 19a), were undertaken near The Rock Hill. AusCover fractional cover estimates, using Landsat acquired on 10 January 2001, gave values of 18 percent bare ground, 41 percent photosynthetic and 40 percent non-photosynthetic vegetation cover in the vicinity of WP62. Fractional cover imagery for the Bulloc Ranges/The Rock Hill shows that the cover is dominated by photosynthetic and to a lesser extent non-photosynthetic vegetation (Hewson 2013). ASD *in situ* field measurements of gravel lag, vegetation and ground litter at WP62 were processed to simulate ASTER ferric oxide content and green vegetation product indices (Table 2) (Figure 20). This limited series of measurements suggested that the presence of dry vegetation matter (*e.g.* lichen, bark, leaf litter) can complicate the ASTER interpretation of ferric iron (*e.g.* hematite, goethite), useful for regolith profile information and/or alteration involving hematitisation (Figure 20). Simulated values for ASTER's AlOH group content index from WP62 gravel lag ASD measurements produced values between 1.9 and 2.15, within the threshold range used to generate ASTER AlOH group content imagery (Cudahy 2012). This compares favourably with the ASTER AlOH group content index value of 2.0 as an average for 2 × 30 m pixels at WP62 extracted from the map product.

5. Conclusions

This study demonstrated, within the test site areas of Mt Fitton and Wagga Wagga, the usefulness of the recently released Australia

Downloaded by [RMIT University] at 15:23 18 February 2015

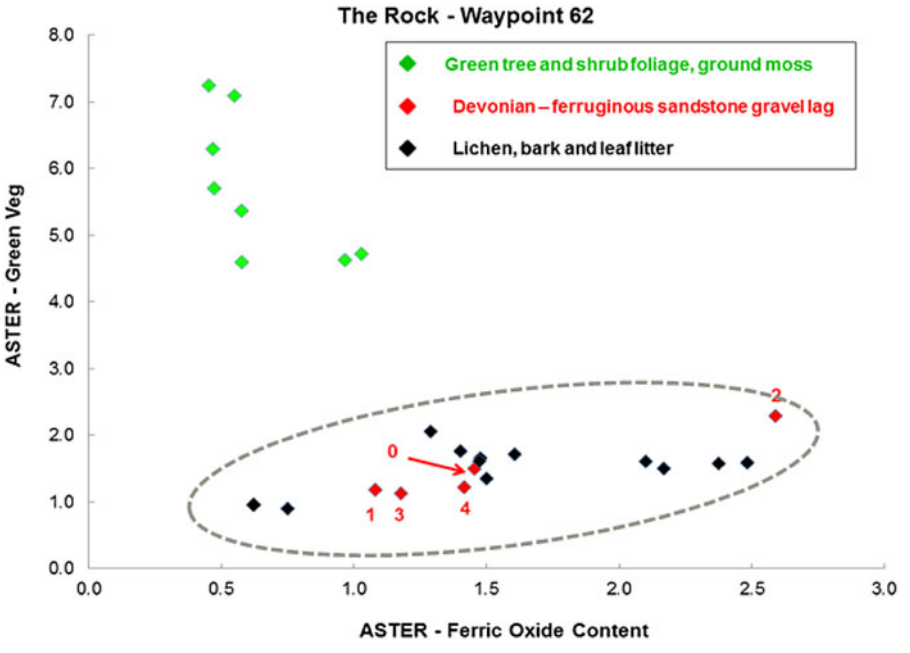


Figure 20. ASD field spectral signatures of vegetation and gravel samples (WP 62), resampled and processed into equivalent ASTER map indices for green vegetation and ferric oxide content.

ASTER map products supplied by CSIRO and GA for identifying or discriminating variations in surface geological composition. These map products included the content and composition of mineral groups within outcropping geological units, possible overprinted alteration and weathered regolith. In particular, many stratigraphic units and areas of mineralised alteration were effectively mapped by the ASTER map products within the Mt Fitton test site. Overall the ASTER map products can potentially aid mineral exploration in Australia within semi-arid areas such as Mt Fitton and, to a lesser extent, within open woodland and cultivated environments such as Wagga Wagga.

Although several ASTER map products provided useful information as individual entities, their application generally benefits geoscience investigations when integrated and interpreted with geophysical, topographical and fractional land cover information. In particular, DEM-derived slope information and vegetation fractional data were found to effectively mask and refine ASTER map products in the vegetated and floodplain-affected Wagga Wagga area. Anomalous AlOH- and silica-rich areas within the Wagga Wagga 100 K map sheet were discriminated and associated with geophysical radiometric and high-frequency filtered TMI inferred features. Radiometric data also appeared to benefit from topographic slope masking to exclude low-relief areas with pervasive alluvial and aeolian transported cover. The application of different data display stretches, such as histogram equalisation, was found to further enhance the display of some anomalous features. The integration of the ASTER map and geophysics products as RGB composites or via 2D scatterplots appears useful for geological interpretation.

Issues of residual ASTER crosstalk within areas of shadow or dark surfaces or dense vegetation, and possible interpretation ambiguities between VNIR derived ferric iron oxide and dry vegetation, highlight the

Downloaded by [RMIT University] at 15:23 18 February 2015

Downloaded by [RMIT University] at 15:23 18 February 2015

importance of validation fieldwork to check anomalous areas. The groundtruthing of the most significant interpreted ASTER anomalies, ideally with a VNIR-SWIR spectrometer, is highly desirable. Further studies into the benefits of integrating acquisition-date relevant AusCover fractional land cover information from Landsat 5 and 7 imagery are recommended for future Australian ASTER applications. The recent successful launch and initial operation of the Landsat 8 sensor, comparable to Landsats 5 and 7, will facilitate future fractional cover estimates planned by TERN. Such multi-temporal land cover information should assist in interpreting future satellite imagery such as from World-View-3 (http://www.digitalglobe.com/about-us/content-collection#worldview-3) and other scheduled missions.

Acknowledgements

This study has been supported and funded by the Geological Survey of NSW, NSW Trade & Investment, in part, for the purpose of contributing to the knowledge of the Wagga Wagga 100,000 map sheet geology for mineral exploration. Geophysical and associated data for the Wagga Wagga and Mt Fitton study areas was received from the Geological Survey of NSW and the Department of Manufacturing, Innovation, Trade, Resources and Energy of SA (DMITRE), respectively. ASTER GeoTIFFs and BSQ ASTER map products were also gratefully obtained from Geoscience Australia and CSIRO-Earth Science & Resource Engineering, whilst the original ASTER imagery was made available by NASA and METI. GIS shapefiles for the Wagga Wagga and Mt Fitton areas were also gratefully obtained from Geoscience Australia. Support from Laurie Buxton of RMIT University was also helpful during this study. Peter Waring and and Malcolm Sheard of DMITRE also provided useful information on the Mt Fitton geology. Simone Meakin of the Geological Survey of NSW has been a great help with editorial and enhancement of illustrations. Matilda Thomas publishes with the permission of the Chief Executive Officer of Geoscience Australia.

References

Caccetta, M., Collings, S., & Cudahy, T. (2013) A calibration methodology for continental scale mapping using ASTER imagery. *Remote Sensing of Environment*, vol. 139, pp. 306–317.

Chen, X.Y. (1997) Quaternary sedimentation, parna, landforms, and soil landscapes of the Wagga Wagga 1: 100 000 map sheet, south-eastern Australia. *Australian Journal of Soil Research*, vol. 35, no. 3, pp. 643–668.

Chen, X.Y., & McKane, D.J. (1997) *Soil Landscapes of the Wagga Wagga 100K Sheet Map and Report*, Department of Land and Water Conservation, Sydney.

Clark, R.N., King, T.V.V., Klejwa, M., Swayze, G., & Vergo, N. (1990) High spectral resolution reflectance spectroscopy of minerals. *Journal of Geophysical Research*, vol. 95, no. B8, pp. 12653–12680.

Coats, R.P., & Blissett, A.H. (1971) Regional and economic geology of the Mount Painter Province. *South Australian Geological Survey Bull*, vol. 43.

Crowley, J.K., Brickey, D.W., & Rowan, L.C. (1989) Airborne imaging spectrometer data of the Ruby Mountains, Montana: mineral discrimination using relative absorption band-depth images. *Remote Sensing of Environment*, vol. 29, no. 2, pp. 121–134.

Cudahy, T.J. (2012), Australian ASTER Geoscience Product Notes, Version 1, 7th August, 2012 – CSIR0, ePublish No. EP-30-07-12-44.

Downes, P.M., McEvilly, R., & Raphael, N.M. (2004) Mineral deposits and models, Cootamundra 1:250,000 map sheet area, *Quarterly Notes, Geoloical Survey of New South Wales* No 116, February, 2004, p37.

Downes, P.M., & Seccombe, P.K. (2008) Sulfur isotope signatures for orogenic gold deposits, Lachlan Orogen, New South Wales, *Proceedings of PACRIM Congress*, 24–26 November, 2008 AusIMM, Gold Coast Qld, Australia.

Duke, E.F. (1994) Near infrared spectra of muscovite, Tschermak substitution, and metamorphic reaction progress: implications for remote sensing. *Geology*, vol. 22, no. 7, pp. 621–624.

Fujisada, H., Sakuma, F., Ono, A., & Kudoh, M. (1998) Design and pre-flight performance of ASTER instrument protoflight model. *IEEE Transactions on Geoscience and Remote Sensing*, vol. 36, no. 4, pp. 1152–1160.

Grove, C.I., Hook, S.J., & Paylor, E.D. II (1992) *Laboratory Reflectance Spectra of 160 Minerals, 0.4 to 2.5 Micrometers*, Jet Propulsion Laboratory, Pasedena, CA, 92–2.

Hewson, R. (2013) Using ASTER and geophysical mapping to assist exploration over Wagga Wagga 1:100,000 sheet area, *Geological Survey*

Downloaded by [RMIT University] at 15:23 18 February 2015

of New South Wales, File GS2013/1558, NSW Department of Trade & Investment, Newcastle, New South Wales, pp. 49.

Hewson, R.D., & Cudahy, T.J. (2011) Issues affecting geological mapping with ASTER data: a case study of the Mt Fitton area, South Australia. *In:* Ramachandran, B., ed. *Land Remote Sensing and Global Environmental Change: NASA s Earth Observing System and the Science of ASTER and MODIS: Applications in ASTER*, Springer-Verlag, New York, ISBN: 978-1-4419-6748-0.

Hewson, R.D., Cudahy, T.J., Drake-Brockman, J., Meyers, J., & Hashemi, A. (2006) Mapping geology associated with manganese mineralisation using spectral sensing techniques at Woodie Woodie, East Pilbara. *Exploration Geophysics*, vol. 37, no. 4, pp. 389–400.

Hewson, R.D., Cudahy, T.J., & Huntington, J.F. (2001) Geologic and alteration mapping at Mt Fitton, South Australia, using ASTER satellite-borne data, *Proceedings of IEEE 2001 International Geoscience and Remote Sensing Symposium (IGARSS)*, 9–13 July, Institute of Electrical and Electronics Engineers, Sydney, New South Wales, pp. 3.

Hewson, R.D., Cudahy, T., Mizuhiko, S., Ueda, K., & Mauger, A.J. (2005) Seamless geological map generation using ASTER in the Broken Hill-Curnamona province of Australia. *Remote Sensing of Environment*, vol. 99, no. 1–2, pp. 159–172.

Hewson, R.D., Cudahy, T.J., Quigley, M., Huntington, J.H., Whitbourn, L.B., & Hausknecht, P. (2003b) Mapping talc mineralisation and associated alteration using airborne and satellite-borne spectrometry: a case study at Mount Fitton, South Australia. Centre for Global Metallogeny, University of Western Australia (Publication 31) / Australian Society of Exploration Geophysics (Special Publication 12) *In:* Dentith, M.C., ed. *Geophysical Signatures of South Australian Mineral Deposits*, Australian Society of Exploration Geophysicists, Perth, Western Australia, pp. 213–221.

Hewson, R.D., Mah, A., Dunne, M., & Cudahy, T.J. (2003a) Mapping Mineralogical and structural relationships with satellite-borne ASTER and airborne geophysics at Broken Hill, *Proceedings of the 16th Geophysical Conference and Exhibition, Australian Society Exploration Geophysicists*, Extended Abstracts, Australian Society of Exploration Geophysicists, Melbourne, Victoria, pp. 3.

Hewson, R., & Robson, D. (2014) Using ASTER and geophysical mapping for mineral exploration in the Wagga Wagga and Cobar areas, N.S.W. *Quarterly Notes of the Geological Survey of New South Wales*, vol. 140, pp. 28.

Hewson, R., Robson, D., Mauger, A., Cudahy, T., Thomas, M., & Jones, S. (2013) Extracting mineralogical and geomorphological information using new ASTER mineral maps with airborne geophysics, *Proceedings of ASEG-PESA 2013, 23rd International Geophysical Conference and Exhibition 2013*, 11–14 August 2013, Australian Society of Exploration Geophysicists, Melbourne, Australia, pp. 4.

Hunt, G.R., & Ashley, R.P. (1979) Spectra of altered rocks in the visible and near infrared. *Economic Geology*, vol. 74, no. 7, pp. 1613–1629.

Iwasaki, A., & Fujisada, H. (2005) ASTER geometric performance. *IEEE Transactions on Geoscience and Remote Sensing*, vol. 43, no. 12, pp. 2700–2706.

Iwasaki, A., Fujisada, H., Akao, H., Shindou, O., & Akagi, S. (2001) Enhancement of spectral separation performance for ASTER/SWIR. *Proceedings of SPIE - The International Society for Optical Engineering*, vol. 4486, pp. 42–50.

Iwasaki, A., & Tonooka, H. (2005) Validation of a crosstalk correction algorithm for ASTER/SWIR. *IEEE Transactions on Geoscience and Remote Sensing*, vol. 43, no. 12, pp. 2747–2751.

Laukamp, C., Cudahy, C., Caccetta, M., Thomas, M., Close, D., & Lennartz, R. (2013) Successful mineral exploration using multispectral remote sensing data - ASTER geoscience map of Australia, *Proceedings 12th SGA Biennial Meeting*, 12–15 August 2013, International Association for Mathematical Geosciences, Uppsala, Sweden, pp. 4.

Lewis, P., & Downes, P.M. (2008) Mineral systems and processes in New South Wales: a project to enhance understanding and assist exploration. *Quarterly Notes, Geoloical Survey of New South Wales*, No 128, April, 2008, pp. 15.

Mars, J.C., & Rowan, L.C. (2010) Spectral assessment of new ASTER SWIR surface reflectance data products for spectroscopic mapping of rocks and minerals. *Remote Sensing of Environment*, vol. 114, no. 9, pp. 2011–2025.

Michael, S. (2012) Satellite imagery: the range and value. *Preview, Australian Society of Exploration Geophysicists*, vol. 160, pp. 20–25.

Raymond, O. (1993) *Wagga Wagga-Kyeamba Region Geological Map 1:100000*, AGSO, Canberra.

Ricchetti, E. (2000) Multispectral satellite image and ancillary data integration for geological

classification. *Photogrammetric Engineering & Remote Sensing*, April, pp. 429–435.

Rowan, L.C., & Mars, J.C. (2003) Lithologic mapping in the Mountain Pass, California area using advanced spaceborne thermal emission and reflection radiometer (ASTER) data. *Remote Sensing of Environment*, vol. 84, no. 3, pp. 350–366.

Salisbury, J.W., & D'Aria, D.M. (1992) Emissivity of terrestrial materials in the 8–14 μm atmospheric window. *Remote Sensing of Environment*, vol. 42, no. 2, pp. 83–106.

Scarth, P., Röder, A., & Schmidt, M. (2010) Tracking grazing pressure and climate interaction - the role of Landsat fractional cover in time series analysis, *Proceedings of the 15th Australasian Remote Sensing and Photogrammetry Conference (ARSPC)*, 13–17 September, Alice Springs, Surveying and Spatial Sciences Institute, Australia.

Sheard, M.J. (2012) MARREE, South Australia, sheet SH54-5, second edition. Geological Atlas 1:250 000 series – explanatory notes, *DMITRE, Mineral and Energy Resources Group. Report Book* 2012/004.

Sherman, D.M. (1985) The electronic structures of Fe3+ coordination sites in iron oxides: applications to spectra, bonding, and magnetism. *Physics and Chemistry of Minerals*, vol. 12, no. 3, pp. 161–175.

van der Meer, F.D., van der Werff, H.M.A., van Ruitenbeek, F.J.A., Hecker, C.A., Bakker, W. H., Noomen, M. F., van der Meijde, M., Carranza, J. M., Smeth, J., & Woldai, T. (2012) Multi- and hyperspectral geologic remote sensing: a review. *International Journal of Applied Earth Observation and Geoinformation*, vol. 14, no. 1, pp. 112–128.

Vincent, R.K., & Thomson, F. (1972) Spectral compositional imaging of silicate rocks. *Journal of Geophysical Research*, vol. 77, no. 14, pp. 2465–2472.

Watanabe, H. (2005) Accuracy of geolocation and DEMfor ASTER, *Proceedings of SPIE, 5978, Sensors, Systems and Next Generation Satellites IX*. International professional society for optics and photonics, Bruges, Belgium.

Yamaguchi, Y., Fujisada, H., Kahle, A., Tsu, H., Kato, M., Watanabe, H., Sato, I., & Kudoh, M. (2001) ASTER instrument performance, operation status, and application to earth sciences, *Proceedings IEEE 2001 International Geoscience and Remote Sensing Symposium*, 9–13 July. Institute of Electrical and Electronics Engineers, Sydney, New South Wales.

Downloaded by [RMIT University] at 15:23 18 February 2015